# Novel Photoplethysmographic Signal Analysis Via Wavelet Scattering Transform*

Agnieszka Szczęsna[1][0000−0002−4354−8258], Dariusz Augustyn[2][0000−0001−7432−3142], Henryk Josiński[1][0000−0003−0196−7777], Adam Świtoński[1][0000−0003−4836−6418], Paweł Kasprowski[2][0000−0002−2090−335X], and Katarzyna Harężlak[2][0000−0003−3573−9772]

[1] Department of Computer Graphics, Vision and Digital Systems, Faculty of Automatic Control, Electronics and Computer Science, Silesian University of Technology, 44-100, Gliwice, Akademicka 16, Poland
agnieszka.szczesna@polsl.pl

[2] Department of Applied Informatics, Faculty of Automatic Control, Electronics and Computer Science, Silesian University of Technology, 44-100, Gliwice, Akademicka 16, Poland

**Abstract.** Photoplethysmography (PPG) is a non-invasive optical technique, applied in clinical settings to measure arterial oxygen saturation. Using modern technology, PPG signals can be measured by wearable devices. This paper presents a novel procedure to study the dynamics of biomedical signals. The procedure uses features of a wavelet scattering transform to classify signal segments as either chaotic or non-chaotic. To this end, the paper also defines a chaos measure. Classification is made using a model trained on a dataset consisting of signals generated by systems with known characteristics. Using an example PPG signal, this paper demonstrates the usefulness of the wavelet scattering transform for the analysis of biomedical signals, and shows the importance of correctly preparing the training set.

**Keywords:** Wavelet Scattering Transform · Chaos · PPG · Classification · Biomedical signals.

## 1 Introduction

Photoplethysmography (PPG) is an non-invasive optical measurement technique. By using a light source to illuminate skin tissue, either the transmitted or reflected light intensity is collected by a photodetector to record the photoplethysmogram. Traditionally, PPG signals have been recorded using red or near infrared light. In recent years, green light has been used for wearable devices, such as wristbands and smartwatches, to provide highly usable and accessible daily health monitoring [12, 8, 10, 16, 31]. As such, a proper understanding of green

* This publication was supported by the Department of Graphics, Computer Vision and Digital Systems, under statue research project (Rau6, 2022), Silesian University of Technology (Gliwice, Poland).

ICCS Camera Ready Version 2022
To cite this paper please use the final published version:
DOI: 10.1007/978-3-031-08757-8_53

light PPG is of critical importance. Recorded light intensity variations have traditionally been associated with blood volume pulsations in the microvascular bed of the tissue. The tissue penetration depth of green light is approximately 530 nm. The source of the chaotic properties of PPG is unclear. Such properties could originate in the upper layers of the skin, due to changes in capillary density caused by arterial transmural pressure, or in deeper layers, due to changes in vessel blood volume [27].

Despite uncertainty concerning the mechanisms of PPG, the technique is generally accepted to provide valuable clinical information about the cardiovascular system. PPG signals are used to monitor pulse rate, heart rate, oxygen saturation, blood pressure, and blood vessel stiffness [28, 15, 17, 13, 2, 22, 23, 21, 7]. Unfortunately, such signals are often corrupted by noise, motion artifacts, and missing data.

Biological signals contain deterministic and stochastic components, both of which contribute to the underlying dynamics of the physiological system. All biological signals contribute information on the underlying physiological processes. Therefore, by studying such signals, the physiological systems that generate them can be better understood.

In early studies, PPG as well as ECG (electrocardiogram) and HRV (heart rate variability) were claimed to be chaotic mostly based on the results of time-delay reconstructed trajectory, correlation dimension and largest Lyapunov exponent [29]. Subsequently, with the development of nonlinear time series analysis methods for real-world data, further evidence of the chaotic nature of such biological signals has emerged. However, many tools that were previously thought to provide clear evidence of chaotic motion have been found to be sensitive to noise and prone to producing misleading results. Thus, controversy remains concerning the topic of chaos in biological signals [11, 26, 27].

Sviridova and Sakai [26] applied nonlinear time series analysis methods to PPG signals to identify the unique characteristics of the underlying dynamical system. Such methods included time delay embedding, largest Lyapunov exponent, deterministic nonlinear prediction, Poincaré section, the Wayland test, and the method of surrogate data. Results demonstrated that PPG dynamics are consistent with the definition of chaotic motion, and the chaotic properties were somewhat similar to Rössler's single band chaos with induced dynamical noise.

A more recent approach to signal analysis is the use of machine learning or deep learning methods. Such methods can generalize knowledge acquired from a training dataset, and apply it to the analysis of a testing dataset. Boullé et al. [3] used a deep neural network to classify univariate time series' generated by discrete and continuous dynamical systems based on the presence of chaotic behavior. The study suggests that deep learning techniques can be used to classify time series' obtained by real-life applications into chaotic or non-chaotic.

De Pedro-Carracedo et al. [9] found that the dynamics of a PPG signal were predominantly quasi-periodic over a small timescale (5000 data points at 250 Hz). Over a longer timescale (600000 data points at 250 Hz), more diverse and

ICCS Camera Ready Version 2022
To cite this paper please use the final published version:
DOI: 10.1007/978-3-031-08757-8_53

complex dynamics were observed, but the signal did not display chaotic behavior. This analysis used a deep neural network to classify the PPG signals. The following dynamics classes were defined: periodic, quasi-periodic, non-periodic, chaotic, and random. Unfortunately, the dataset used to train the network contained only one system for each class. Given that chaotic systems are difficult to generalize [6], this is not sufficient to accurately classify the dynamics of the real-life signal.

De Pedro-Carracedo et al. [20] applied a modified 0–1 test to the same PPG time series' as the above study. They also found that the majority of PPG signals displayed quasi-periodic behavior across a small timescale, and that as the timescale increased the dynamics became more complex, due to the introduction of additional cardiac rhythm modulation factors. Under specific physiological conditions, such as stress, illness, or physical activity, a transition from quasi-periodicity to chaos can be possible. This phenomenon provides the motivation for measuring the presence of chaos within PPG signals under various conditions.

The objective of this study is to analyze the dynamics of PPG signals during different everyday activities. We propose a novel approach to classify signals using features of a wavelet scattering transform (WST) and a support vector machine (SVM) classifier. This approach was simplified by defining only two classes of signals: chaotic and non-chaotic. Compared to previous research, the training data was prepared in greater detail, and included noise, which was omitted in previous works.

Wavelet analysis provides a unifying framework for the description of many time series phenomena [25]. Introduced by Mallat [18], WST has a similar architecture to convolutional neural network. Despite requiring no parameter learning, WST performs strongly, particularly in constrained classification tasks. WST is a cascade of complex wavelet transforms and modulus non-linearities. At a chosen scale, averaging filters provide invariance to shifts and deformations within signals [1]. Hence, WST can be applied accurately and efficiently to small datasets, whereas convolutional neural network require a large amount of training data. Consequently, WST features possess translation invariance, deformation, stability, and high-frequency information [4]. As such, WST is highly suitable feature extractors for non-linear and non-stationary signals, and has been widely used in audio, music, and image classification.

Moreover, WST is often used to analyze time series', including biomedical signals. By inputting WST features to an SVM classifier, electroencephalography signals were correctly classified as belonging to alcoholic or non-alcoholic patients [5]. In addition, a WST was used to classify heart beats based on ECG signals, with an accuracy of 98.8–99.6%. Jean Effil and Rajeswari [14] used a WST and a deep learning long short-term memory algorithm to accurately estimate blood pressure from PPG signals.

ICCS Camera Ready Version 2022
To cite this paper please use the final published version:
DOI: 10.1007/978-3-031-08757-8_53

## 2 Materials and methods

### 2.1 The Wavelet Scattering Transform

The wavelet transform is convolutions with dilated wavelets. For 2D transformations, the wavelets are also rotated. Being localized waveforms, wavelets are stable to deformations, unlike Fourier sinusoidal waves. A scattering transform creates nonlinear invariants using wavelet coefficients with modulus and averaging pooling functions. Such transforms yield representations that are time-shift invariant, robust to noise, and stable to time-warping deformations. These attributes are highly useful for many classification tasks, and wavelet transforms are the most common method applied to limited datasets. Andén and Mallat [1] provide a brief overview of the key properties of scattering transforms, including stability to time-warping deformation and energy conservation, and describe a fast computational algorithm.

The WST consists of three cascading stages. In the first stage, the signal $x$ undergoes decomposition and convolution with a dilated mother wavelet $\psi$ of center frequency $\lambda$, giving $x*\psi_\lambda$. Following this, the convolved signal is subjected to a nonlinear modulus operator, which typically increases the signal frequency and can compensate for the loss of information due to down sampling. Finally, a time-average/low-pass filter in the form of a scaling function $\phi$ is applied to the absolute convolved signal, giving $|x * \psi_\lambda| * \phi$.

The zero-order scattering coefficients $S_0$ describe the local translation invariance of the signal:

$$S_0 = x * \phi.$$

At each level, the averaging operation causes the high-frequency parts of the convolved signal to be lost. These parts can be recovered via the convolution of the signal with the wavelet in the following level.

The first-order scattering coefficients $S_1$ are therefore defined as the average absolute amplitudes of wavelet coefficients for any scale $1 \leq j \leq J$, over a half-overlapping time window of size $2^j$:

$$S_1 = |x * \psi_{\lambda_1}| * \phi.$$

The second-order scattering coefficients $S_2$ are calculated by repeating the above steps:

$$S_2 = ||x * \psi_{\lambda_1}| * \psi_{\lambda_2}| * \phi.$$

The higher order wavelet scattering coefficients can be calculated by iterating the above process.

The scattering coefficients for each level of the wavelet scattering transform are obtained by processing the defined constant-$Q$ filter bank, where $Q$ is the number of wavelets per octave. Each level can have a filter bank with different $Q$ parameters.

During implementation we used the MATLAB (version R2021b) *waveletScattering* function. The two-layer WST was obtained using Gabor wavelet. For the first and second levels $Q_1 = 8$ and $Q_2 = 1$ respectively. The transform is invariant

ICCS Camera Ready Version 2022
To cite this paper please use the final published version:
DOI: 10.1007/978-3-031-08757-8_53

to translations up to the invariance scale, which is set to half of the signal length in the default implementation. The scaling function determines the duration of the invariant in time. Moreover, the invariance scale affects the spacing of the wavelet center frequencies in the filter banks. The output $R^{paths \times windows \times signals}$ is a feature tensor. This tensor was reshaped into a matrix which is compatible with the SVM classifier. The columns and rows of the matrix correspond to scattering paths and scattering time windows respectively. This results in a feature matrix of $signals \cdot windows$ rows and $paths - 1$ columns.

The zero-order scattering coefficients are not used. Given that multiple scattering windows are obtained for each signal, repeated labels were created that corresponded to the labels (0, 1). Following this, normalization was applied. Scattering coefficients of order greater than 0 were normalized by their parents along the scattering path. Using the defined parameters for the $N$ input signals (runs), each composed of 1000 samples, this procedure produced a $102 \times 8 \times N$ WST feature tensor, which was then transformed into a $N \cdot 8 \times 101$ matrix.

### 2.2 Classification model

The testing and training datasets were created using 13 dynamical systems (five chaotic and eight non-chaotic) of first, second, or third order. Table 1 shows the training set characteristics. Each system was provided with 1000 created test files, each of which contained 1000 samples. Augmentation was applied by randomizing the initial conditions, defined by the $\mathbf{x}_0$ vector, according to the formula $[2 \cdot rand() - 1] \cdot \mathbf{x}_0$, where $rand()$ generates pseudorandom numbers that are uniformly distributed in the interval $(0, 1)$. The chaotic systems are represented by driven or autonomous dissipative flows. Previously described as A.4.5, A.5.1, A.5.2, A.5.13, and A.5.15 [24], we describe these flows as CHA_1,CHA_2, CHA_3, CHA_4, and CHA_5, respectively. The non-chaotic systems were divided into the following classes: i) periodic, including the OSC_1, OSC_2, DOSC_1, and IOSC systems; ii) quasi-periodic, including QPS_1 and QPS_2; and iii) non-periodic, including DS_1 and DS_2. The quasi-periodic systems are described by the general function

$$x = f(t) = A_1 \cdot sin(\omega_1 \cdot t + \varphi_1) + A_2 \cdot sin(\omega_2 \cdot t + \varphi_2),$$

where the ratio $\omega_1/\omega_2$ is irrational.

Based on previous PPG signal analysis, we made the following experimental design choices:

- A signal with a length of 1000 samples was obtained from each system using 1000 runs with different initial parameters. Each dimension of the multi-dimensional systems was treated separately. This corresponded to analysis using windows with a short time horizon of 31.2 s for the 32 Hz PPG signal.
- We used SVM classification with a radial basis kernel similar to that proposed by Buriro et al. [5]. The classification is made based on WST features.
- Two classes were defined for the classification task: chaotic (class 1) and non-chaotic (class 0). The decision to use just two classes, and therefore fold

ICCS Camera Ready Version 2022
To cite this paper please use the final published version:
DOI: 10.1007/978-3-031-08757-8_53

periodic, quasi-periodic, and non-periodic behavior into the same class, was made to test the thesis that PPG signals are never chaotic [9]. In further work, a larger number of more distinct classes will be used.
– Sviridova and Sakai [26] show that PPG signals display some similarity to Rössler's chaos with induced dynamical noise. As such, we used Rössler's system as one of the signals with chaotic behavior, as shown in Figure 1. Furthermore, all signals with additive white Gaussian noise were added to the whole set.

The accuracy of the trained models was checked by 10-fold cross-validation.

To investigate the properties of the training set, the following models were trained:

– *Model01* was trained without output signals from Rössler's system (CHA_3). Using 10-fold cross-validation, accuracy was validated as 100%. Testing using Rössler's system signal showed 32% accuracy. Based on the model, it is impossible to effectively classify the signals produced by chaotic systems. It is therefore important to include the signals from CHA_3 within the training set.
– *Model02* was trained without the quasi-periodic systems QPS_1 and QPS_2. Using 10-fold cross-validation, accuracy was validated as 100%. Testing using QPS_1 and QPS_2 showed 78.5% accuracy. On this basis, we determine that quasi-periodic systems are easier to correctly classify.
– *Model03* was trained on signals without additional noise. Using 10-fold cross-validation, accuracy was validated as 100%. Testing using signals with additive Gaussian noise with a signal to noise ratio of 7dB showed 94.03% accuracy. Although the analytical methods for the assessment of chaotic behavior are highly sensitive to noise, the prepared model is not, and even noisy signals can be classified with high accuracy.
– *Model01N* and *Model02N* are variants of models *Model01* and *Model02* respectively, trained additionally with noisy signals.
– *ModelAll* was trained using all signals, both with and without additive Gaussian noise, with a signal to noise ratio of 7dB. Using 10-fold cross-validation, accuracy was validated as 99.88%.

### 2.3 PPG dataset

The dataset used in this work is the public available PPG dataset for motion compensation and heart rate estimation in daily life activities (PPG-DaLiA[3]) [21]. Given that the database contains a reference ECG measurement, it is often used to test heart rate estimation algorithms [31]. The dataset contains a total of 36 hours of recording for 15 study participants undertaking eight different types of physical everyday life activities: working, sitting, walking, eating lunch, driving, cycling, playing football, and climbing stairs. The sensor data was obtained from commercially available devices. In our case, the 64 Hz PPG signals

[3] https://ubicomp.eti.uni-siegen.de/home/datasets/sensors19/, accessed July 2021

ICCS Camera Ready Version 2022
To cite this paper please use the final published version:
DOI: 10.1007/978-3-031-08757-8_53

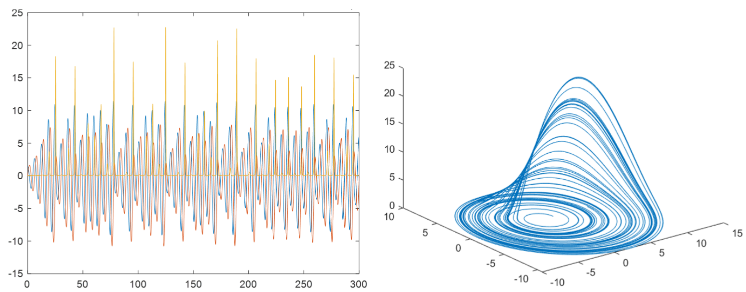

Fig. 1: 3D signals and a phase portrait of the Rössler system (CHA_3).

Table 1: The training set characteristics.

| Name and symbol | Class | Dimension | Short description |
|---|---|---|---|
| Ueda oscillator CHA_1 | chaotic (class 1) | 2 | driven dissipative flow |
| Lorenz attractor CHA_2 | chaotic (class 1) | 3 | autonomous dissipative flow |
| Rössler attractor CHA_3 | chaotic (class 1) | 3 | autonomous dissipative flow |
| Halvorsen's cyclically symmetric attractor CHA_4 | chaotic (class 1) | 3 | autonomous dissipative flow |
| Rucklidge attractor CHA_5 | chaotic (class 1) | 3 | autonomous dissipative flow |
| Undamped oscillator 1 OSC_1 | periodic (class 0) | 2 | slow oscillations with constant amplitude |
| Undamped oscillator 2 OSC_2 | periodic (class 0) | 2 | fast oscillations with constant amplitude |
| Damped oscillator 1 DOSC_1 | periodic (class 0) | 2 | fast oscillations with decreasing amplitude |
| Oscillator with increasing amplitude of oscillations IOSC | periodic (class 0) | 2 | oscillations with growing amplitude |
| Damped system 1 DS_1 | non-periodic (class 0) | 3 | slow fading signals |
| Damped system 2 DS_2 | non-periodic (class 0) | 3 | fast fading signals |
| Quasi-periodic system 1 QPS_1 | quasi-periodic (class 0) | 1 | irrational ratio: $\omega_1/\omega_2 = \pi$ |
| Quasi-periodic system 2 QPS_2 | quasi-periodic (class 0) | 1 | irrational ratio: $\omega_1/\omega_2 = (1+\sqrt{5})/2$ |
| 16 000 000 samples | 0 | | all samples of signals with non-chaotic behavior |
| 16 000 000 samples | 1 | | all samples of signals with chaotic behavior |

which we used for testing the trained models were recorded by the wrist-worn Empatica E4 device.

The base frequency of the PPG signals was adjusted to match the training set. We counted the number of signal zero crossings within a given time interval when using the $CHA\_5$ system. We were required to increase the frequency of zero crossings by a factor of two, giving a final PPG signal frequency of 32 Hz.

## 3 Results

The PPG signal was split into 1000 samples (31.2 s) segments, following fitting and resampling. For each segment, the WST features were obtained. As part of the analysis, the signal was split into $W = 8$ scattering windows of 125 samples each. A classification result was generated for each scattering window. The overall classification of a segment is the ratio of the number of windows classified as having chaotic behavior (class 1), to the total number of windows. Hence, a segment that contains eight chaotic windows represents a fully chaotic segment of signal. Within the overall signal, we define the chaotic measure to be the ratio of chaotic windows to total number of windows. Tests were conducted for all models, as shown in Table 2. Figures 2 and 3 present the PPG signal and the value of the chaotic measure for each segment.

ICCS Camera Ready Version 2022
To cite this paper please use the final published version:
DOI: 10.1007/978-3-031-08757-8_53

Table 2: Results for all tested models—the ratio of windows classified as chaotic to the total number of windows within the PPG signal. The highest values for each model have been marked.

| Participant | *Model01* | *Model01N* | *Model02* | *Model02N* | *Model03* | *ModelAll* |
|---|---|---|---|---|---|---|
| *S01* | 0.27 | 0.07 | 0.25 | 0.14 | 0.26 | 0.11 |
| *S02* | 0.29 | 0.12 | 0.28 | 0.15 | 0.29 | 0.15 |
| *S03* | 0.22 | 0.07 | 0.17 | 0.12 | 0.19 | 0.09 |
| *S04* | 0.30 | 0.16 | 0.28 | 0.20 | 0.29 | 0.19 |
| *S05* | **0.56** | **0.33** | **0.53** | **0.34** | **0.54** | **0.33** |
| *S06* | 0.26 | 0.11 | 0.21 | 0.14 | 0.23 | 0.13 |
| *S07* | 0.42 | 0.13 | 0.36 | 0.20 | 0.40 | 0.17 |
| *S08* | 0.23 | 0.11 | 0.22 | 0.14 | 0.23 | 0.13 |
| *S09* | 0.27 | 0.14 | 0.26 | 0.18 | 0.26 | 0.18 |
| *S10* | 0.23 | 0.10 | 0.22 | 0.12 | 0.22 | 0.13 |
| *S11* | 0.47 | 0.25 | 0.44 | 0.28 | 0.46 | 0.26 |
| *S12* | 0.20 | 0.07 | 0.16 | 0.11 | 0.17 | 0.09 |
| *S13* | 0.50 | 0.22 | 0.44 | 0.26 | 0.47 | 0.24 |
| *S14* | 0.22 | 0.06 | 0.16 | 0.11 | 0.17 | 0.08 |
| *S15* | 0.18 | 0.06 | 0.14 | 0.10 | 0.16 | 0.08 |

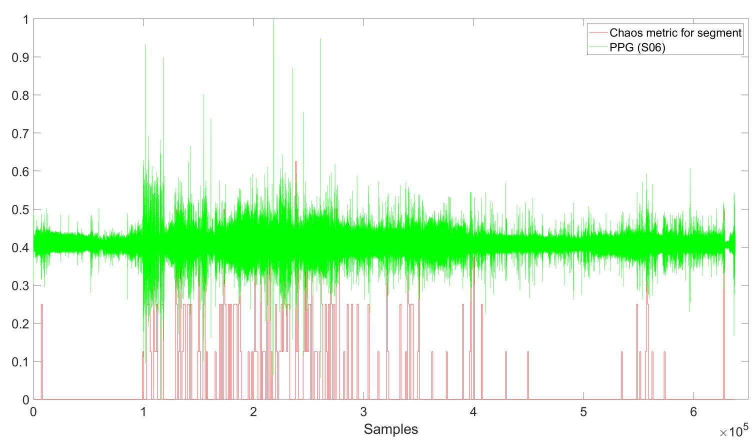


Fig. 2: Chaos measure values when using *ModelAll*, for each 1000 sample segment for the *S06* participant.

ICCS Camera Ready Version 2022
To cite this paper please use the final published version:
DOI: 10.1007/978-3-031-08757-8_53

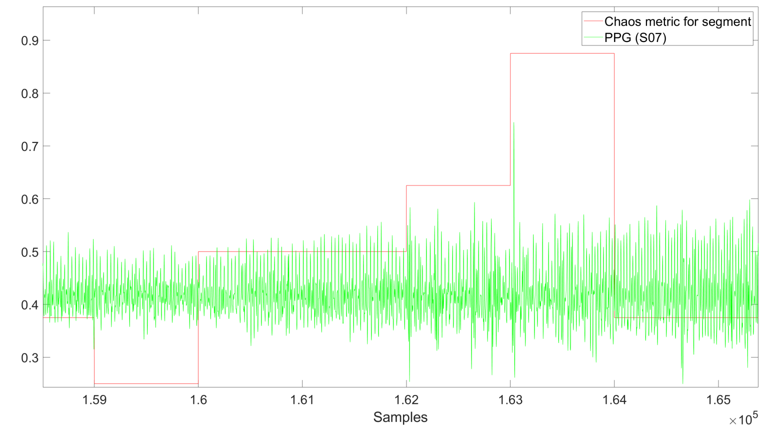


Fig. 3: Chaos measure values when using *ModelAll*, for each 1000 sample segment for a fragment of the PPG signal of the *S07* participant.

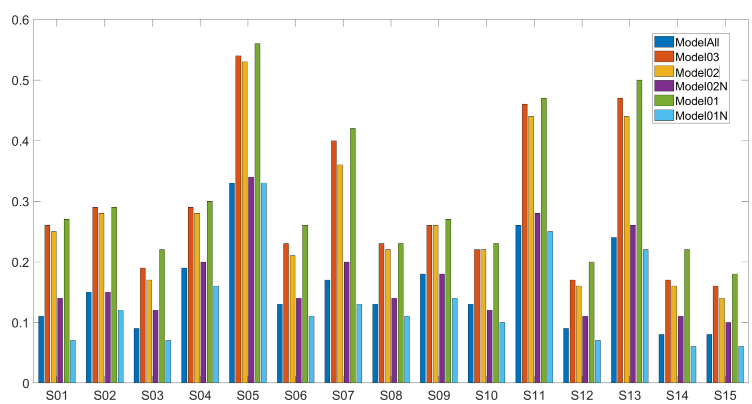


Fig. 4: Chaos measure values for each participant.

ICCS Camera Ready Version 2022
To cite this paper please use the final published version:
DOI: 10.1007/978-3-031-08757-8_53

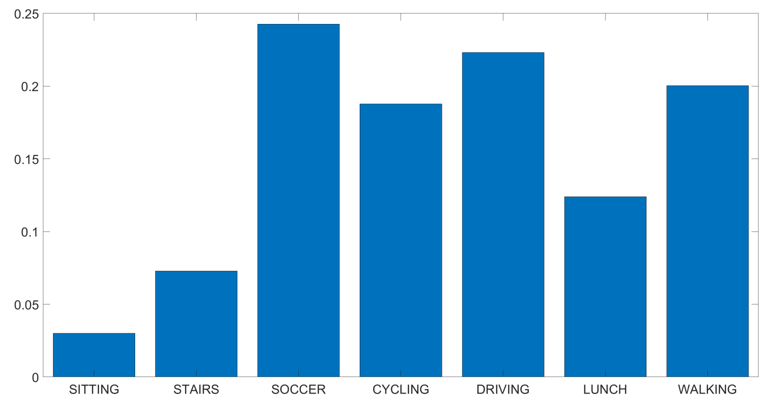


Fig. 5: Average chaos measure values for each activity.

The results show that those models trained without additional noise—*Model01*, *Model02*, and *Model03*—display high chaotic measure values (see Figure 4). The differences between each of these models are not significant. This confirms that noise is present within the data, and is highly relevant to its evaluation.

Those models that were trained with additional noise—*Model01N*, *Model02N*, and *ModelAll*—display greater differences in the chaotic measure. *Model01N* produced the lowest values of chaotic measure, meaning that fewer segments were classified as exhibiting chaotic behavior. Hence, the PPG signals display some similarity to the Rössler system. *Model02N* produced the highest values of chaotic measure, showing that a model trained without quasi-periodic functions classifies such behavior as chaotic. Moreover, the inclusion of such a class of functions was justified. *ModelAll* produces results between those of *Model01N* and *Model02N*.

The highest values of chaotic measure, independent of the model used, were obtained from the PPG signal of participant *S05*. Interestingly, this participant reported the greatest errors in heart rate estimation using deep neural networks. The mean heart rate was significantly higher than for all other participants [31, 21].

Figure 5 shows that the greatest values of chaotic measure are obtained during the cycling, soccer, driving, and walking activities. The values differ between activities, indicating that the measure is influenced by movement or changes in heart rate as a result of physical activity, stress, or the general condition and health of the participant. The relationship is not well defined, as the participants had the highest heart rate when climbing stairs and cycling. Further analysis of this phenomenon is required.

The calculations were performed on the computer with the following parameters: Windows 10, Intel(R) Core(TM) i7-7700HQ CPU 2.80GHz, 32GB, Matlab R2021b. The biggest differences in training and classification times are

ICCS Camera Ready Version 2022
To cite this paper please use the final published version:
DOI: 10.1007/978-3-031-08757-8_53

between the models based signals without noise and with additional noisy signals. The average time of determining WST features for models *Model_01*, *Model_02*, *Model_03* is 14.55956667 s (std 0.996971916), the training time is 19.45903333 s (std 2.239389959), and the average classification time of one window is 0.000109 s (std 0.000061). Taking into account the models *Model_01N*, *Model_02N*, *Model_All* the average times are as follows: WST features calculations - 42.526825 s (std 4.489965561), training - 289.576025 s (std 21.05237103), classifications - 0.000435 s (std 0.000044).

## 4 Conclusions

The results show that signal classification based on system features requires careful preparation of the training set. Chaotic systems create signals that are difficult to predict. Therefore, insufficient data within the training set may cause misclassification. The noise within real measured signals must also be accounted for.

Furthermore, a WST can be used to successfully determine signal features for the purpose of classification. Given that such wavelet analysis is well understood, parameters can be chosen straightforwardly. Moreover, the training model is supposed to be much faster than the use of deep learning methods, which is worth future investigation.

The analysis showed that PPG signals display chaotic features over short time spans. The measure of chaos is dependent upon the activity performed. Given that wearable devices are easily available and are increasingly used for medical diagnosis [30, 19], understanding this phenomenon is highly important and the topic requires further detailed analysis.

The aim of this study was to demonstrate the usefulness of WST for the analysis of biomedical signals, and to show the importance of correctly preparing the training set. Interest in the classification of real signals by deep learning methods is increasing; such methods may lead to erroneous conclusions if the training sets are inadequately prepared.

## References


1. Andén, J., Mallat, S.: Deep scattering spectrum. IEEE Transactions on Signal Processing **62**(16), 4114–4128 (2014)
2. Biswas, D., Simões-Capela, N., Van Hoof, C., Van Helleputte, N.: Heart rate estimation from wrist-worn photoplethysmography: A review. IEEE Sensors Journal **19**(16), 6560–6570 (2019)
3. Boullé, N., Dallas, V., Nakatsukasa, Y., Samaddar, D.: Classification of chaotic time series with deep learning. Physica D: Nonlinear Phenomena **403**, 132261 (2020)
4. Bruna, J., Mallat, S.: Invariant scattering convolution networks. IEEE transactions on pattern analysis and machine intelligence **35**(8), 1872–1886 (2013)
5. Buriro, A.B., Ahmed, B., Baloch, G., Ahmed, J., Shoorangiz, R., Weddell, S.J., Jones, R.D.: Classification of alcoholic eeg signals using wavelet scattering transform-based features. Computers in Biology and Medicine **139**, 104969 (2021)


ICCS Camera Ready Version 2022
To cite this paper please use the final published version:
DOI: 10.1007/978-3-031-08757-8_53

6. Chen, Z., Xiu, D.: On generalized residual network for deep learning of unknown dynamical systems. Journal of Computational Physics **438**, 110362 (2021)
7. Chung, H., Ko, H., Lee, H., Lee, J.: Feasibility study of deep neural network for heart rate estimation from wearable photoplethysmography and acceleration signals. In: 2019 41st Annual International Conference of the IEEE Engineering in Medicine and Biology Society (EMBC). pp. 3633–3636. IEEE (2019)
8. Coughlin, S.S., Stewart, J.: Use of consumer wearable devices to promote physical activity: a review of health intervention studies. Journal of environment and health sciences **2**(6) (2016)
9. De Pedro-Carracedo, J., Fuentes-Jimenez, D., Ugena, A.M., Gonzalez-Marcos, A.P.: Is the ppg signal chaotic? IEEE Access **8**, 107700–107715 (2020)
10. Friel, C.P., Garber, C.E.: An examination of the relationship between motivation, physical activity, and wearable activity monitor use. Journal of Sport and Exercise Psychology **42**(2), 153–160 (2020)
11. Glass, L.: Introduction to controversial topics in nonlinear science: Is the normal heart rate chaotic? Chaos: An Interdisciplinary Journal of Nonlinear Science **19**(2), 028501 (2009)
12. Hannan, A.L., Harders, M.P., Hing, W., Climstein, M., Coombes, J.S., Furness, J.: Impact of wearable physical activity monitoring devices with exercise prescription or advice in the maintenance phase of cardiac rehabilitation: systematic review and meta-analysis. BMC Sports Science, Medicine and Rehabilitation **11**(1), 1–21 (2019)
13. Ismail, S., Akram, U., Siddiqi, I.: Heart rate tracking in photoplethysmography signals affected by motion artifacts: a review. EURASIP Journal on Advances in Signal Processing **2021**(1), 1–27 (2021)
14. Jean Effil, N., Rajeswari, R.: Wavelet scattering transform and long short-term memory network-based noninvasive blood pressure estimation from photoplethysmograph signals. Signal, Image and Video Processing **16**(1), 1–9 (2022)
15. Kamshilin, A.A., Nippolainen, E., Sidorov, I.S., Vasilev, P.V., Erofeev, N.P., Podolian, N.P., Romashko, R.V.: A new look at the essence of the imaging photoplethysmography. Scientific reports **5**(1), 1–9 (2015)
16. Kossi, O., Lacroix, J., Ferry, B., Batcho, C.S., Julien-Vergonjanne, A., Mandigout, S.: Reliability of actigraph gt3x+ placement location in the estimation of energy expenditure during moderate and high-intensity physical activities in young and older adults. Journal of Sports Sciences pp. 1–8 (2021)
17. Kumar, A., Komaragiri, R., Kumar, M., et al.: A review on computation methods used in photoplethysmography signal analysis for heart rate estimation. Archives of Computational Methods in Engineering pp. 1–20 (2021)
18. Mallat, S.: Understanding deep convolutional networks. Philosophical Transactions of the Royal Society A: Mathematical, Physical and Engineering Sciences **374**(2065), 20150203 (2016)
19. Manninger, M., Kosiuk, J., Zweiker, D., Njeim, M., Antolic, B., Kircanski, B., Larsen, J.M., Svennberg, E., Vanduynhoven, P., Duncker, D.: Role of wearable rhythm recordings in clinical decision making—the wehrables project. Clinical cardiology **43**(9), 1032–1039 (2020)
20. de Pedro-Carracedo, J., Ugena, A.M., Gonzalez-Marcos, A.P.: Dynamical analysis of biological signals with the 0–1 test: A case study of the photoplethysmographic (ppg) signal. Applied Sciences **11**(14), 6508 (2021)
21. Reiss, A., Indlekofer, I., Schmidt, P., Van Laerhoven, K.: Deep ppg: Large-scale heart rate estimation with convolutional neural networks. Sensors **19**(14), 3079 (2019)


ICCS Camera Ready Version 2022
To cite this paper please use the final published version:
DOI: 10.1007/978-3-031-08757-8_53

22. Salehizadeh, S., Dao, D., Bolkhovsky, J., Cho, C., Mendelson, Y., Chon, K.H.: A novel time-varying spectral filtering algorithm for reconstruction of motion artifact corrupted heart rate signals during intense physical activities using a wearable photoplethysmogram sensor. Sensors **16**(1), 10 (2016)
23. Schäck, T., Muma, M., Zoubir, A.M.: Computationally efficient heart rate estimation during physical exercise using photoplethysmographic signals. In: 2017 25th European Signal Processing Conference (EUSIPCO). pp. 2478–2481. IEEE (2017)
24. Sprott, J.C.: Chaos and time-series analysis, vol. 69. Oxford University Press (2003)
25. Staszewski, W., Worden, K.: Wavelet analysis of time-series: coherent structures, chaos and noise. International Journal of Bifurcation and Chaos **9**(03), 455–471 (1999)
26. Sviridova, N., Sakai, K.: Human photoplethysmogram: new insight into chaotic characteristics. Chaos, Solitons & Fractals **77**, 53–63 (2015)
27. Sviridova, N., Zhao, T., Aihara, K., Nakamura, K., Nakano, A.: Photoplethysmogram at green light: Where does chaos arise from? Chaos, Solitons & Fractals **116**, 157–165 (2018)
28. Tamura, T.: Current progress of photoplethysmography and spo 2 for health monitoring. Biomedical engineering letters **9**(1), 21–36 (2019)
29. Tsuda, I., Tahara, T., Iwanaga, H.: Chaotic pulsation in human capillary vessels and its dependence on the mental and physical conditions. In: Proceedings of the Annual Meeting of Biomedical Fuzzy Systems Association: BMFSA 4. pp. 1–40. Biomedical Fuzzy Systems Association (1992)
30. Vandecasteele, K., De Cooman, T., Gu, Y., Cleeren, E., Claes, K., Paesschen, W.V., Huffel, S.V., Hunyadi, B.: Automated epileptic seizure detection based on wearable ecg and ppg in a hospital environment. Sensors **17**(10), 2338 (2017)
31. Wilkosz, M., Szczęsna, A.: Multi-headed conv-lstm network for heart rate estimation during daily living activities. Sensors **21**(15), 5212 (2021)


ICCS Camera Ready Version 2022
To cite this paper please use the final published version:
DOI: 10.1007/978-3-031-08757-8_53